IDENTIFICATION OF DISTORTIONS TO FBG SPECTRUM USING FBG FIXED FILTERS"

G.C. Kahandawa*, J. A. Epaarachchi, H. Wang
Centre of Excellence in Engineered Fibre Composites
University of Southern Queensland, Australia

* Corresponding author (gayan@usq.edu.au)

Keywords: *FBG Sensors, Composite materials, Structural Health Monitoring*

1 Introduction

Recent advances in fibre optic sensor technologies have provided great opportunities to develop more sophisticated in-situ SHM systems. There have been a large number of research reports on health monitoring of composite structures using Fibre Bragg Grating (FBG) sensors. Distortion of FBG sensors has been successfully used by many researchers to identify damage and to locate damage in composite structures [1]. Observations of the distorted sensor spectrums due to stress concentrations caused by delaminations and cracks, have been using to estimate the damage conditions. The majority of the research works were focused on the investigation of the spectra of a FBG sensor embedded in the vicinity of a damage, in order to detect and identify the damage by relating to the distortion of the FBG sensor spectra.

However the cause of the distortion of FBG spectra not only depends on the consequences of accumulated damage but also loading types and the fibre orientation. Embedding FBG's in-between non parallel fibre layers and the application of torque have caused substantial distortions to the FBG spectra [2]. A reference FBG spectra needs to be incorporated to FBG measurements to identify the variations to the FBG spectrum and to distinguish the other effects causing distortions. For this purpose, a fixed FBG based system was developed to measure the reflected FBG spectra in time domain. The fixed FBG method was used to estimate the peak using non distorted FBG spectra previously [3]. Unfortunately there was no work done on the identification of distortions of FBG spectra using fixed FBG sensors.

This paper details the research work performed to identify distortions of reflected spectra of an embedded FBG sensors inside a composite laminate. The developed method will provide the flexibility of input FBG time domain data directly to post processing algorithms for decoding and damage identification.

1.1 Distortion of the FBG sensor spectrum

The majority of research work on FBG sensors in SHM of composite structures were focused on investigation of the spectrums of FBG sensor embedded in the vicinity of damage. Observations of the distorted sensor spectrums due to stress concentrations caused by delaminations and cracks, been used to estimate the damage conditions. Takeda and co-workers have investigated purposely damaged axially loaded specimens. The changes of FBG spectra were attributed to the damage and successfully reconstructed spectrum using the strain-field data [1]. In real life situations, the applied loads are not limited to uni-axial loads and hence the performance of FBGs in multi-axial loading situation needs to be investigated for complete understanding of damage status. The FBG spectral response is significantly complicated under multi-axial loading conditions [4]. The distortion of FBG spectra not only depend on the consequences of accumulated damage but also the loading types [5]. Recently, it has been shown that the embedding FBG's in-between non parallel fibre layers and the application of torque have caused substantial distortions to the FBG spectra [2]. Fig 1 provides a simple explanation to this discrepancy. The pressure load applied on FBG sensor by the outer glass fibre layers, can distort the circular cross section of FBG to an oval shape. Since the FBG sensor is placed in-between non-parallel fibre layers, micro bending of the sensor is also possible. The top 90^o layer fibres undergo tension due to the torsional loading on the tube. Due to the large diameter of the FBG sensor,

compared to the diameter of glass fibres, there are additional transverse forces on the FBG sensors which lead to a micro bending as shown in Fig 2.
Both these effects will lead to a variation of the refractive index of the core material, causing the distorted spectrum. The variation of Bragg wave length λ_B, as a function of change in the refractive index $\Delta\delta n$, and the grating period $\delta\Lambda_o$, is given below.

$$\delta\lambda_{Bragg} = 2\Lambda_o\eta\Delta\delta n + 2n_{eff}\delta\Lambda_o \quad (1)$$

Where η is core overlap factor of ~0.9 times the shift of Bragg wavelength [6]. This explanation also supports the observations reported in [7] and [8].
This paper details a developed spectral decoding system to overcome these discrepancies.

1.2 Theoretical Background

System for decoding FBG Spectrum using fixed FBG filters been developed by several researchers [9, 10] and the system we used is shown in the Fig 3. There were several attempts to fit the curves using mathematical functions and one of the common used is the Gaussian curve fit. Sensor reflectivity can be expressed as

$$S(\lambda, \lambda_s) = y_o + S_o \exp[-\alpha_s(\lambda - \lambda_s)^2] \quad (2)$$

Where y_o is the added offset to represent the dark noise, as α is a parameter related to full width at half maximum (FWHM) and λ is the wave length.

Unfortunately Gaussian fit always gives an error for a distorted spectrum as shown in Fig 4.a. Only the individual segments of the distorted FBG spectra provide a measure of distortion. As such distorted spectrum must consider as a piece wise continuous function, f_{pc} in order to capture the distortion caused to FBG spectra (Fig 4.b). Consequently, optical power, P of the distorted signal can be obtained as:

$$P = \beta \sum_{i=1}^{N} P_i \quad (3)$$

β is the constant depend on the power of the source, P_i the area covered under the distorted spectra in the time limit between t_a and t_b. Apparently P_i at each point is proportional to the strain (Fig 4.b).

2 Methodology

2.1 Sample fabrication

Two FRP panels (Specimen 1 and 2) were fabricated with UD glass fibres and Kenetix R246TX resin as the matrix. The lay-up configuration is 0/0/90/90/0/0 for Specimen 1 and the Specimen 2 is 0/+45/-45/-45/+45/0.
FBG sensors within the range of 1550 nm centre wavelength were fabricated on 9um core and 125um clad diameter telecommunication grade glass fibre. The grading length is 10mm. To ensure maximum bonding between FBG sensor and matrix of resin in the GFRP material, the acrylate layer of the fibre was removed. Extra protective layer of rubber was applied in the fibre to maximise the handling of samples without damage to the sensors. In both panels the FBG sensor was placed in-between outer layers. In Specimen 2 in between 0/0 layers and in Specimen 3 between 0/+45 layers.

2.2 Fixed FBG Sensors

A FBG sensor at 1567.29 nm, a photo diode (PD) and two fibre optic couplers were arranged as in Fig 3. The reflected spectrum from the FBG1 sensor is input to the fixed external FBG2 filter which is with α=1.6 through the couplers. Consequently, the intersection of the two spectrums will be output by the PD. The signal is captured by the high speed data acquisition system (DAQ) which is connected to the PD.
The reflected light of the filter was captured by the PD and the resulting PD voltage was recorded using the DAQ. Fig 4.(a) shows the PD voltage in the time domain corresponding to the intersection of the spectrums shown in the Fig 4.(b). Tuneable laser frequency allows recording the voltage reading directly in the time domain. Since the filter spectra is fixed, the intersection of the two spectra is only depends on the sensor spectrum position. Variation of the intersection has been used to estimate the location of the peak and then the strain at sensor. Furthermore, any distortion to the spectrum is visible from the PD voltage-time plot. By matching the tuneable laser swept frequency with the DAQ sampling frequency, it is possible to estimate the wavelength values accurately. More details can be found in Ref [10].

In this work one FBG was used to cover the operational wavelength range. However multiple FBGs will be needed to cover a wider operating range of the FBG sensor.

2.3 Testing

A lateral pressure of 6MPa was applied on the embedded FBG sensors in Specimens 1 and 2 by means of a load of 2250 N applied on an area of 25 X 15 mm as shown in Fig 5 and spectrums were recorded using the OSA.

Subsequently, the specimens were loaded using a mechanically operated testing machine as shown in Fig 6. The panels were subjected to a torque and axial load independently and subsequent combined axial and torsional loads. The machine used to apply axial tension to the specimen by moving top and bottom supports. The torque was applied on the other hinge by means of a handle fixed to one support while the other support is fixed. The rotating handle is shown in Fig 6 (b). Initially, Specimen 1 was subjected to a 10 Nm torque without axial load, and with axial loads of 420 N and 730 N, the same 10 Nm toque was applied. The FBG spectrum was recorded for three load cases, namely pure axial, pure torsion and combined loading.
Next the specimens were uni-axially loaded up to 1800N. In each 100 N increment PD voltage was recorded by the attached DAQ in the time domain. The FBG spectral response was also recorded using Micron Optics sm125 Optical Spectrum Analyzer (OSA) (in wavelength domain) for verification purposes.

3. Results and discussion

Specimen 1 with an FBG in between layers 1 and 2, both with 0^o fibre direction, did not show any significant distortion to the spectrum under lateral pressure loading as shown in Fig 7.
There is no or minimal possibility of micro bending happened in the FBG sensor since the glass fibre and FBG are parallel to each other. The spectrum of FBG in Specimen 2 in between layers 1 and 2, which are in 45^o angle to each other, was distorted as shown in Fig 8, under lateral pressure loading. The overlapping glass fibre applying individual small transverse forces on the FBG, as explained above in the section 1.1, could possibly be the cause for this behavior.
Fig 9 shows the distortion of the spectrum of the FBG sensor embedded in Specimen 1 due to applied torque of 10 Nm only. Fig 10 and 11 shows the distortion of FBG spectrum with 420N and 730N axial load combined with the 10 Nm torque.
The peak of the spectrum moved smoothly rightwards with the applied axial load. While the axial load is fixed at 420 N, torque of 10 Nm was applied on the specimen. The spectrum distorted as shown in the Fig 10. The peak of the spectrum moved leftward, while axial load remains at 420 N. The process was repeated with a higher axial load, 730 N and the results obtained were similar as shown in Fig 11.

Specimen 1 is with an embedded FBG sensor in between parallel glass fibre layers. By twisting the panel the FBG also gets twisted, but the possibility of micro bending is minimal. Hence the results obtained in Fig 9, 10 and 11 representing the twisting effect on FBG and it has been observed that the use of FBG sensors to measure axial strain in a twisted sample is not accurate.
To capture the distortion of the FBG spectra observed in lateral and torsional loading, the fixed FBG was used. The distortion of the FBG responses observed by the OSA at each load level are depicting in the Fig 12. The intersection of embedded and the fixed FBG spectrums which was captured by the PD (Fig 13) undoubtedly shows that the distortions of the spectra can be directly measured using the decoder (PD) output.

4. Conclusions

The distortions to the FBG spectrum was successfully captured using fixed FBG sensor arrangement. A discrete segment of the distorted spectra has been isolated by fixed FBG sensors. The area of the distorted segments is proportional to the strain and hence the time domain data can be converted to strain or directly input to any SHM system. Further investigations are warranted to optimize number of fixed FBG sensors in a filter to capture the fine details of the distortion.

References

[1] S. Takeda. Y.Okabe. N. Takeda, "Monitoring of delamination growth in CFRP laminates using chirped FBG sensors." *Journal of Intelligent Material Systems and Structures*, Vol 19, no 4, 2008.

[2] G.C. Kahandawa. J.A. Epaarachchi. H. Wang. J. Canning, "Effects of the self distortions of embedded FBG sensors on spectral response due to torsional and combined loads", *Proceedings of APWSHM3*, Tokyo, 2010.

[3] A.C. Zimmentmann. C.L.N. Veiga and L.S. Encinas, "Unambiguous signal processing and measuring range extension for fibre bragg grating sensors using artificial neural networks-Temperature case", *IEEE sensors*, Vol. 8, No 7, 2008.

[4] L. Sorensen. J. Botsis. T. Gmur. J. Cugnoni, "Delamination detection and characterisation of bridging tractions using long FBG optical sensors", *Composites*, 2007.

[5] G.C. Kahandawa. J.A. Epaarachchi. H. Wang. D. Followell. P. Birt J. Canning and M. Stevenson, "An investigation of spectral response of embedded Fibre Bragg Grating (FBG) sensors in a hollow composite cylindrical beam under pure torsion and combined loading", ", *Proceedings of ACAM 6*, Perth, Australia, 2010.

[6] R. Kashyap, "*Fibre Bregg gratings*", Academic Press Publications, 1999

[7] C. Martelli. J. Canning. B. Gibson. S. Huntington, "Bend loss in structured optical fibres", *Optical Society of America*, Vol 15, No 26, 2007.

[8] S. Mastro, "Optomechanical behavior of Bragg Grating sensors under transverse load", SEM Proceedings, 2005.

[9] L.C.S. Nunes. L.C.G. Valente. A.M.B. Braga, "Analysis of a demodulation system for Fiber Bragg Grating sensors using two fixed filters", Optics and Lasers in Engineering, 2004.

[10] L.C.S Nunes. B.S. Olivieri. C.C. Kato. L.C.G. Valente and A.M.B. Braga, "FBG sensor multiplexing system based on the TDM and fixed filter approach", Sensors and Actuators, 2007.

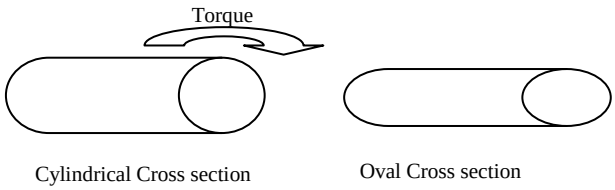

Fig.1. Twist of the sensor due to torsional loading

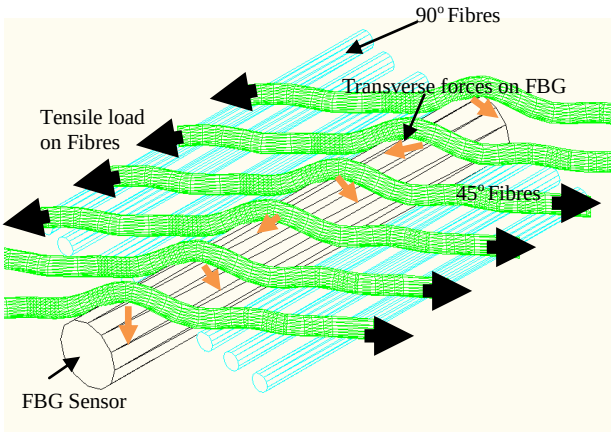

Fig.2. Transverse loading on FBG sensor

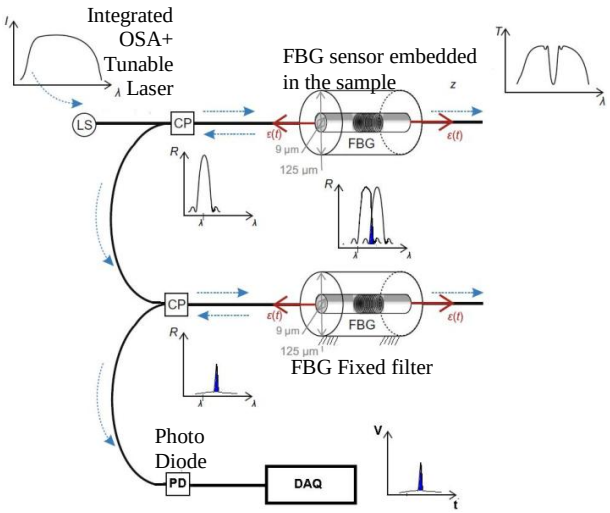

Fig.3. FBG spectrum decoding system

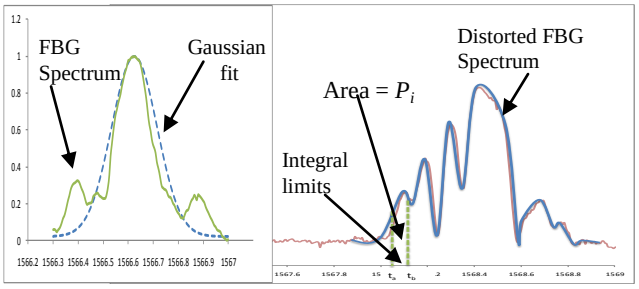

Fig.4. (a) Gaussian fit (b) Piecewise continuous function

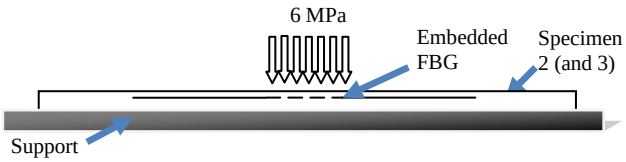

Fig.5. Lateral loading of FBG sensor in Specimen 1 and 2

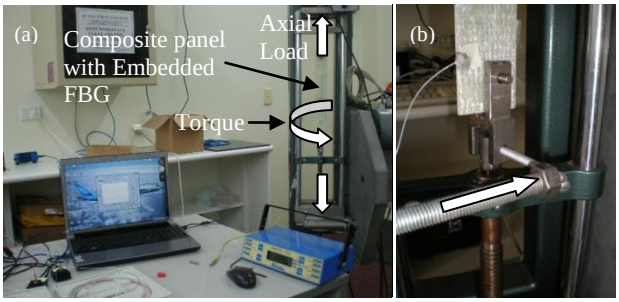

Fig.6. Axial and torsional loading on FBG

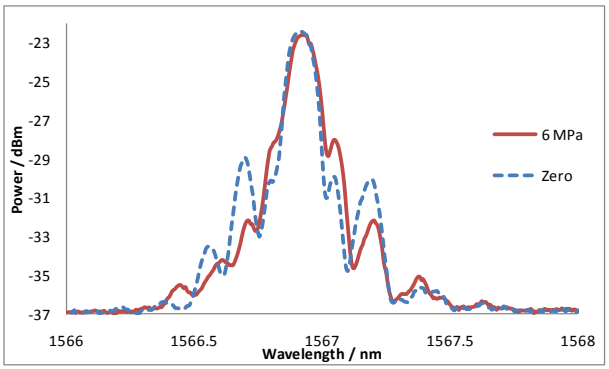

Fig.7. Distortion in the FBG sensors in specimen 1 due to lateral loading

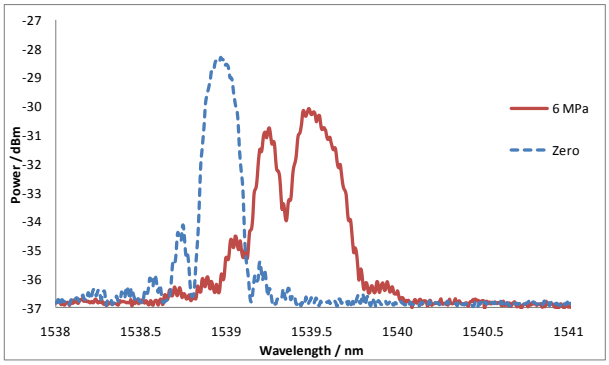

Fig.8. Distortion in the FBG sensor in Specimen 2 due to lateral loading

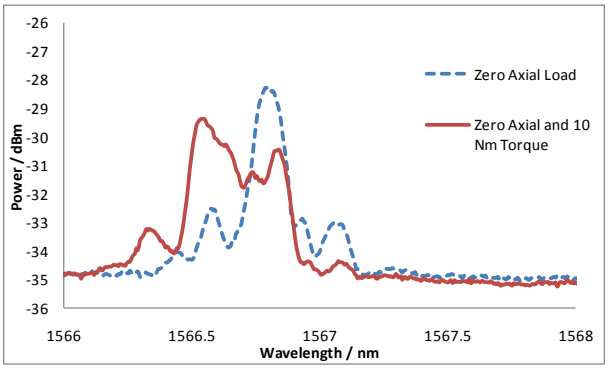

Fig.9. Spectra of embedded FBG in Specimen 3 under an applied torque.

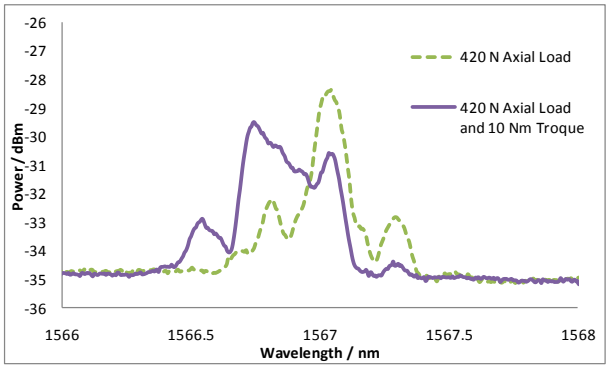

Fig.10. Spectra of embedded FBG in Specimen 1 under 420 N axial and 10 Nm torsional Load.

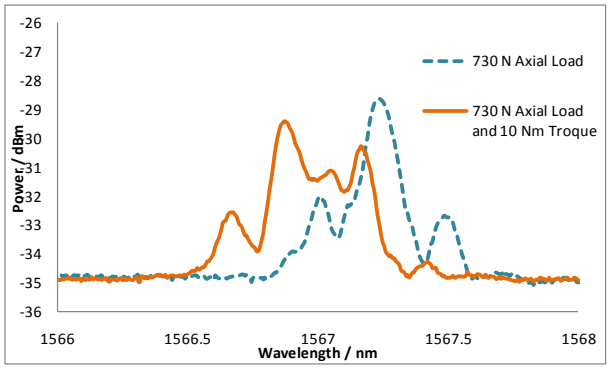

Fig.11. Spectra of embedded FBG in Specimen 1 under 730 N axial and 10 Nm torsional Load.

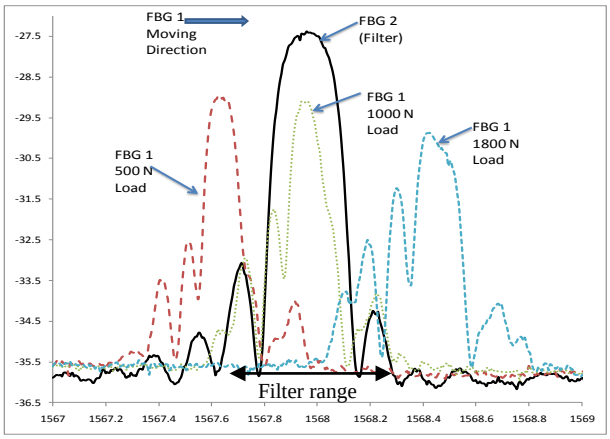

Fig.12. Responses of the sensor and the filter

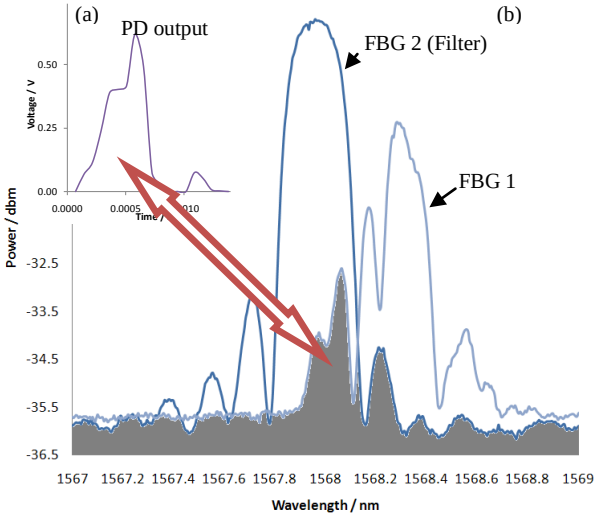

Fig.13. Intersection of the FBG spectra and the PD reading at 1550N